Functional coupling of diverse voltage-gated Ca 2+ channels underlies high- fidelity of fast dendritic Ca 2+ signals during burst firing

Nadia Jaafari, Marco Canepari

J Physiol, in press

Functional coupling of diverse voltage-gated Ca^{2+} channels underlies high-fidelity of fast dendritic Ca^{2+} signals during burst firing

Running title: Functional coupling of voltage-gated Ca^{2+} channels
Keywords: Calcium channels, back propagating action potential, neuronal dendrites
Table of contents category: Neuroscience

Nadia Jaafari[1,2,3] and **Marco Canepari**[1,2,3]

[1] Laboratory for Interdisciplinary Physics, UMR 5588, Université Grenoble 1 and CNRS, 38402 Saint Martin d'Hères, France. [2] Institut National de la Santé et Recherche Médicale (INSERM), France. [3] Laboratories of Excellence, Ion Channel Science and Therapeutics, France.

Corresponding author: Marco Canepari, Laboratoire Interdisciplinaire de Physique, Bat. E45, 140 avenue de la physique, 38402 St Martin d'Hères cedex, France. Email: marco.canepari@ujf-grenoble.fr

Number of characters in the title: 134
Number of characters in the running title: 50
Number of words in the Key points summary: 148
Number of words in the abstract: 234
Number of figures: 10
Number of tables: 1

Key points

- In neurons, the Ca^{2+} signal associated with the dendritic backpropagating action potential codes a chemical message to the different dendritic sites, playing a crucial role in electrical signalling, synaptic transmission and synaptic plasticity.
- The study of the underlying Ca^{2+} current, mediated by different types of voltage-gated Ca^{2+} channels, cannot be achieved by using the patch clamp technique.
- In this article, we used a recently developed cutting-edge optical technique to investigate the physiological behaviour of local Ca^{2+} currents along the apical dendrite of CA1 hippocampal pyramidal neurons.
- We directly measure, for the first time, the synergistic activation and de-activation of the diverse dendritic voltage-gated Ca^{2+} channels operating during bursts of back-propagating action potentials to precisely control the Ca^{2+} signal.
- We demonstrate that the Ca^{2+} loss *via* high-voltage activated channels is compensated by the Ca^{2+} *via* the other channels translating in high-fidelity of Ca^{2+} signalling.

Abstract

In CA1 hippocampal pyramidal neurons, the dendritic Ca^{2+} signal associated with somatic firing represents a fundamental activation code for several proteins. This signal, mediated by voltage-gated Ca^{2+} channels (VGCCs), varies along the dendrites. In this study, using a recent optical technique based on the low-affinity indicator Oregon Green 488 BAPTA-5N, we analysed how activation and de-activation of VGCCs produced by back-propagating action potentials (bAPs) along the apical dendrite shape the Ca^{2+} signal at different locations in CA1 hippocampal pyramidal neurons of the mouse. We measured, at multiple dendritic sites, the Ca^{2+} transients and the changes in membrane potential associated with bAPs at 50 µs temporal resolution and we estimated the kinetics of the Ca^{2+} current. We found that during somatic bursts, the bAPs decrease in amplitude along the apical dendrite but the amplitude of the associated Ca^{2+} signal in the initial 200 µm dendritic segment does not change. Using a detailed pharmacological analysis, we demonstrate that this effect is due to the perfect compensation of the loss of Ca^{2+} *via* high voltage-activated (HVA) VGCCs by a larger Ca^{2+} component *via* low voltage-activated (LVA) VGCCs, revealing a mechanism coupling the two VGCCs families K^+ channels. More distally, where the bAP doesn't activate HVA-VGCCs, the Ca^{2+} signal is variable during the burst. Thus, we demonstrate that HVA- and LVA-VGCCs operate synergistically to stabilise Ca^{2+} signals associated with bAPs in the most proximal 200 µm dendritic segment.

Abbreviations

bAPs, back-propagating action potentials; HVA, high voltage-activated; I_{Ca}/Vol, Ca^{2+} current to volume ratio; LVA, low voltage-activated; OG5N, Oregon Green 488 BAPTA-5N; VGCCs, voltage-gated Ca^{2+} channels; $\Delta F/F_0$, fractional change of fluorescence.

Introduction

The fast elevation of dendritic Ca^{2+} concentration (Ca^{2+} transient) associated with the backpropagating action potential (bAP), in different neuronal systems, is important for several dendritic functions (Waters *et al.* 2005), including the shaping and transmission of synaptic signals (Bloodgood & Sabatini, 2006; Wang *et al.* 2014), the induction of synaptic plasticity (Frick *et al.* 2004), the generation of distal Ca^{2+} spikes (Larkum *et al.* 1999), the dendritic release of neurotransmitters (Isaacson, 2001), the release of endocannabinoids (Wilson *et al.* 2001; Navarrete & Araque, 2010) and the synthesis of nitric oxide (Li *et al.* 2014). This signal is mediated by diverse dendritic voltage-gated Ca^{2+} channels (VGCCs) (Magee *et al.* 1998) and codes different information at different time scales to several target proteins. The Ca^{2+} transient associated with a single bAP precisely activates fast-binding proteins within a short time window after each somatic action potential. In contrast, a persistent Ca^{2+} transient associated with multiple-spike firing is expected to activate mainly slower proteins. In neocortical and hippocampal pyramidal neurons, the bAP declines along the main apical dendrite (Williams & Stuart, 2000; Spruston *et al.* 1995). Both in the neocortex (Markram *et al.* 1995) and in the hippocampus (Christie *et al.* 1995), in the proximal part of the dendrite, the Ca^{2+} transient is mediated by high-voltage activated (HVA) VGCCs (L-type, N-type and P/Q-type), low-voltage activated (LVA) VGCCs (T- type) and R-type VGCCs which open at an intermediate membrane potential (V_m). More distally, where the bAP becomes smaller, the Ca^{2+} transient is mediated only by R-type and T-type VGCCs (Christie *et al.* 1995; Magee & Johnston, 1995) and no Ca^{2+} transient is evoked in many terminal branches. However, a short burst of action potentials can produce dendritic regenerative events in CA1 hippocampal pyramidal neurons (Andreasen & Lambert, 1995), and Ca^{2+} spikes in the tuft of neocortical layer-5 (Larkum *et al.* 1999) and layer-6 (Laderberger & Larkum, 2010) pyramidal neurons. Thus, the Ca^{2+} transients associated with the single action potential and with the burst will likely code different information proximally and distally along the apical dendrite.

To uncover the mechanisms that underlie this remarkable spatio-temporal specialisation in dendritic Ca^{2+} signalling, this study addresses the fundamental question on how the different VGCCs activate and de-activate during the different modes of firing activity to shape the Ca^{2+} transient in CA1 hippocampal pyramidal neurons. We performed Ca^{2+} imaging experiments at ultrafast time resolution (50 µs/frame) using the low affinity indicator Oregon Green 488 BAPTA-5N (K_d = 35 µM, Canepari & Ogden, 2006).

Whereas Ca^{2+} measurements using high-affinity indicators (with K_d < 1 µM) distort the physiological Ca^{2+} transients, (Canepari & Mammano, 1999; Higley & Sabatini, 2008), the use of low affinity indicators (with K_d > 10 µM) allows physiological measurements of Ca^{2+} transients. In addition, the equilibration of the Ca^{2+} binding reaction for low affinity indicators is generally more rapid than the kinetics of a Ca^{2+} influx and the kinetics of the Ca^{2+} current can be obtained by calculating the time derivative of the fluorescence change (Sabatini & Regehr, 1998). Utilising this principle, we recently developed a method to accurately measure the kinetics of the Ca^{2+} current from relatively small sub-cellular compartments (Jaafari *et al.* 2014; 2015). Here, we applied this method to measure the activation and de-activation of VGCCs during bAPs along the apical dendrite. These events are locally regulated by the V_m waveform that changes in the various dendritic sites. To correlate the dynamics of VGCCs with the V_m waveform at each site of recording, we combined Ca^{2+} measurements with optical V_m measurements using voltage sensitive dyes. We focussed on how activation and de-activation of the different VGCCs change when the V_m waveform also changes, in particular during physiological bursts of action potentials. We discovered that HVA-VGCCs and LVA-VGCCs operate in synergy to stabilise the Ca^{2+} elevation associated with bAPs when these V_m waveforms change and we discuss the functional consequence of this phenomenon.

Methods

Slice preparation, solutions and electrophysiology

The general experimental procedures were described in a previous report (Jaafari *et al.* 2104). Briefly, experiments performed at the Laboratoire Interdisciplinaire de Physique were approved by the Isere prefecture (Authorisation n. 38 12 01) and the specific protocol (n. 197) by the ethics committee of the Grenoble Institute of Neuroscience. Hippocampal slices (250 µm thick) were prepared from 21-35 postnatal days old C57Bl6 mice (of both genders) using a Leica VT1200 (Leica, Wetzlar, Germany). Slices were cut in iced extracellular solution and incubated at 37°C for 1 hr before use. The extracellular solution used contained (in mM): 125 NaCl, 26 $NaHCO_3$, 1 $MgSO_4$, 3 KCl, 1 NaH_2PO_4, 2 $CaCl_2$ and 20 glucose, bubbled with 95% O_2 and 5% CO_2. The intracellullar solution contained (in mM): 125 $KMeSO_4$, 5 KCl, 8 $MgSO_4$, 5 Na_2-ATP, 0.3 Tris-GTP, 12 Tris-Phosphocreatine, 20 HEPES, adjusted to pH 7.35 with KOH.

The Ca^{2+} indicator Oregon Green 488 BAPTA-5N (OG5N, Invitrogen, Carlsbad, CA) was added at the concentration of 2 mM. In voltage-imaging experiments, cells were pre-loaded with the voltage-sensitive dye JPW1114 (Invitrogen, Carlsbad, CA) at a concentration of 120 µg/mL, incubated for ~1h and re-patched as described in a previous methodological report (Canepari *et al.* 2008). All recordings were performed at 32-34°C. Toxins were purchased from Smartox (St Martin d'Hères, France). All other chemicals were purchased either from Tocris (Bristol, UK) or Sigma-Aldrich (St. Louis, MO). Experiments were performed at 32-34°C using an Olympus BX51 microscope equipped with a 60X/1.0 NA Nikon objective. Patch-clamp recordings were made using a Multiclamp amplifier 700A (Molecular Devices, Sunnyvale, CA) and voltage and current signals were acquired with the A/D board of the CCD camera. The V_m measured with the patch pipette was corrected for the junction potential (-11 mV) as previously estimated (Canepari *et al.* 2010). Full names of chemical used to block L-type, N-type and T-type VGCCs were Isradipine: 4-(2,1,3-Benzoxadiazol-4-yl)-1,4-dihydro-2,6-dimethyl-3,5-pyridinecarboxylic acid methyl 1-methylethyl ester; PD173212: *N*-[[4-(1,1-Dimethylethyl)phenyl]methyl-*N*-methyl-L-leucyl-*N*-(1,1-dimethylethyl)-*O*-phenylmethyl)-L-tyrosinamide; ML218: 3,5-dichloro-*N*-[[(1α,5α,6-exo,6α)-3-(3,3-dimethylbutyl)-3-azabicyclo[3.1.0]hex-6-yl]methyl]-benzamide-hydrochloride; NNC550396: (1*S*,2*S*)-2-[2-[[3-(1*H*-Benzimidazol-2-yl)propyl]methylamino]ethyl]-6-fluoro-1,2,3,4-tetrahydro-1-(1-methylethyl)-2-naphthalenyl-cyclopropanecarboxylate-dihydrochloride. Full names of chemical used to block glutamate receptors were NMDA: *N*-Methyl-D-aspartic acid; DL-AP5: DL-2-Amino-5-phosphonopentanoic acid.

Optical recordings

Ca^{2+} and V_m optical measurements were achieved sequentially (Canepari *et al.* 2007; Canepari & Vogt, 2008) by alternating excitation of the Ca^{2+} indicator at 470 nm with an OptoLED (CAIRN Research Ltd., Faversham, UK) and the voltage sensitive dye at 532 nm using a 300 mW solid state laser (model MLL532, CNI, Changchun, China). The Ca^{2+} fluorescence was recorded at 510 ± 42 nm and the V_m fluorescence at >610 nm using a NeuroCCD-SMQ camera (RedShirtimaging, Decatur, GA). Simultaneous Ca^{2+} and V_m optical measurements using the voltage sensitive dye JPW1114 could be in principle obtained using either Fura Ca^{2+} indicators (Vogt *et al.* 2011a) or Oregon Green Ca^{2+} indicators and blue illumination to excite V_m fluorescence (Jaafari *et al.* 2014). In neither of those two approaches, however, the high signal-to-noise ratio (S/N) necessary to perform distally the Ca^{2+} measurement or the V_m

measurement cannot be achieved. Images, de-magnified by ~0.1X to visualise ~300 µm, were acquired at 20 kHz with a resolution of 26 X 4 pixels. At least 35 minutes after establishing the whole cell configuration was necessary to guarantee that Ca^{2+} fluorescence was nearly stable in the most proximal 200 µm of the apical dendrite and that Ca^{2+} fluorescence from all recording regions was clearly distinguishable from the background. In more distal dendrites dye equilibration may occur over a longer time scale (Yasuda *et al.* 2004). Nevertheless, quantitative analyses requiring comparisons of optical data from distal dendrites acquired over longer periods were not critical for any of the conclusions reported in this study. Optical signals associated with bursts elicited by somatic current injection of 25 ms were from single trials. In all other experiments, 9-16 trials were averaged to improve the S/N after carefully checking the exact temporal matching of the somatic electrical signal in each trial to verify their consistency. Finally, fluorescence averages were corrected for bleaching using filtered trials without signal.

Analysis of optical data

All data were analysed with Matlab (The Mathworks, Natick, MA). Ca^{2+} and V_m data were initially expressed as fractional changes of fluorescence ($\Delta F/F_0$ signals), calculated after subtraction of the autofluorescence background. The Ca^{2+}-$\Delta F/F_0$ signal associated with each bAP, normalised to its asymptotic value, was initially fitted with a 3-sigmoid function Y(t):

$$Y(t) = \prod_{j=1}^{3} \frac{1}{1+e^{-\varphi_j \cdot (t-\theta_j)}}$$

where t is time and φ_j and θ_j are the parameters to be determined by the fit (Jaafari *et al.* 2015). The time derivative of the fitted Ca^{2+}-$\Delta F/F_0$ signal was then expressed as percentage change over milliseconds (%/ms). The fit was always performed over a time window of 3-5 ms. Under this condition, the fit of the second and the third Ca^{2+}-$\Delta F/F_0$ signal along a burst was never affected by the small decay of the previous Ca^{2+} transient. The previous calibration (Jaafari *et al.* 2014) in Ca^{2+} current to volume ratio (I_{Ca}/Vol in pA/µm^3) was not used here since it was based on measurements performed only in the very initial part of the apical dendrite using 1 mM OG5N. The V_m $\Delta F/F_0$ signal was calibrated in terms of V_m change on an absolute scale using a previously demonstrated protocol, based on wide-field photorelease of L-glutamate (Vogt *et al.* 2001b). The halfwidth of all signals reported here is the interval during which the signal is above 50% of its peak.

Statistics

The significance of the changes produced by addition of a channel blocker was assessed by performing a student t-test. The correlation between two parameters was assessed calculating the Pearson linear coefficient. The probabilities associated with the two tests (either $p < 0.01$ or $p < 0.05$) were reported when a significant change of a variable or a significant correlation was found.

Results

Ca^{2+} transients and currents associated with single action potentials

To investigate the kinetics of the Ca^{2+} current associated with bAPs, we analysed the Ca^{2+} transient in 109 CA1 hippocampal pyramidal neurons. The approach to obtain the kinetics of the Ca^{2+} current consists in recording Ca^{2+} fluorescence from Oregon Green 488 BAPTA-5N at 50 µs time resolution, to calculate the fractional change of fluorescence ($\Delta F/F_0$), to fit the $\Delta F/F_0$ curve with a model function and to calculate the time derivative of the fit, referred in the text as Ca^{2+} current to volume ratio or "I_{Ca}/Vol" signal. We performed all Ca^{2+} measurements over a segment of ~300 µm corresponding to 70-90% of the main apical dendrite and we focussed the analysis in each cell on three sample regions: a proximal (P) region, within 100 µm from the soma; a medial (M) region, between 100 and 200 µm from the soma; and a distal (D) region, beyond 200 µm from the soma as shown in the example of Fig. 1*A*. The model function used to fit the $\Delta F/F_0$ curve in the three sample regions was a 3-sigmoid function as described elsewhere (Jaafari *et al.* 2015) and in the Methods. The accuracy of this procedure to derive the precise kinetics of the Ca^{2+} current relies on the match between the $\Delta F/F_0$ signal and the fit, as illustrated in Fig. 1*B*.

To understand how the different VGCCs activate and de-activate during the bAP, it is necessary to measure the concomitant V_m waveform associated with the bAP at the site of the Ca^{2+} signal. To this purpose, we combined the Ca^{2+} measurement with the V_m optical measurement using the voltage sensitive dye JPW1114, as described in the Methods. In these experiments, we also applied a previously described calibrating procedure (Vogt *et al.* 2011b) to estimate the depolarisation associated with the bAP at all recording sites. Since the attenuation of the bAP is variable from cell to cell (Spruston *et al.* 1995; Migliore *et al.* 1999; Golding *et al.* 2001; Canepari *et al.* 2007), we show in Fig. 2*A*-*B* two examples in

which we observed a different degree of attenuation. In the example reported in Fig. 2*A*, the action potential propagated with relatively weak attenuation along the apical dendrite. In this case, a relatively large Ca^{2+} transient was observed along the entire dendritic segment recorded, but the distal I_{Ca}/Vol peak was smaller than that in the proximal and medial regions. In contrast, in the example of Fig. 2*B*, the action potential attenuated more strongly along the apical dendrite resulting in a more rapid decrease of the Ca^{2+} transient and of the associated I_{Ca}/Vol signal, in particular in the distal region. In all regions, the peak of the I_{Ca}/Vol signal was delayed by 400-600 µs (8-12 frames) reflecting the time necessary for activation and de-activation of VGCCs. The profiles of the bAP peak, of the $\Delta F/F_0$ peak, of I_{Ca}/Vol peak and of the I_{Ca}/Vol halfwidth in the 18 neurons tested are reported in Fig. 2*C*. The attenuation of the bAP along the proximal and medial dendrite was generally moderate, as also reported in a previous study (Vogt *et al.* 2011b). Thus, in these regions, the associated I_{Ca}/Vol signals associated with the bAP had typically peak > 2%/ms and halfwidth < 1ms (Fig. 2*C*). In the distal dendrites, where the attenuation of the bAP was stronger, the I_{Ca}/Vol signal had, in most of the cases, peak < 2%/ms and halfwidth > 1ms (Fig. 2*C*). As shown in Fig. 3*A*, the halfwidth of I_{Ca}/Vol, was negatively correlated with the peak of the action potential (Pearson coefficient $\rho = -0.70$, $p < 0.01$). The I_{Ca}/Vol halfwidth was always shorter in the proximal dendrite with respect to the distal dendrite. In the example of Fig. 3*B*, the bAP and the associated I_{Ca}/Vol were normalised and aligned to their peaks. In the proximal dendrite, the Ca^{2+} current was different in kinetics with respect to the bAP, an evidence observed in all 18 cells. In contrast, in the distal dendrite, the bAP and the I_{Ca}/Vol waveform had very similar kinetics (Fig. 3*B*). Altogether, data presented in Fig. 2 and Fig. 3 represents the first direct measurement of the bAP and of the associated physiological Ca^{2+} current along the majority of an apical dendrite. The interval between the bAP and the Ca^{2+} current can be explained by the expected delay of activation of VGCCs. The different shape of the Ca^{2+} current in the proximal and distal dendrites (Fig. 3*B*) can be explained by the different VGCCs activated. Indeed, as reported in Christie *et al.* 1995, the larger bAP in the proximal and medial dendrites activate both HVA- and LVA-VGCCs whereas the smaller bAP in the distal dendrite can activate only T-type and R-type VGCCs. Thus, in the proximal dendrite, the Ca^{2+} current component mediated by HVA-VGCCs would activate at $V_m > -30$ mV and would have shorter duration with respect to the bAP. In contrast, in the distal dendrite, the dominant component mediated by LVA-VGCCs would be activated during the entire supra-threshold depolarisation and would have a similar waveform with respect to the V_m signal.

Although the activation of different VGCCs in proximal and distal dendrites is an established result, the hypothesis that this is the cause of the different kinetics in the different dendritic sites required a direct confirmation. Thus, we performed a detailed pharmacological analysis on the Ca^{2+} current, as shown in the examples of Fig. 4. The five different types of VGCCs where selectively blocked as follows:

L-type → 20 µM Isradipine (*Isr*)

N-type → 5 µM PD173212 (*PD*)

P/Q-type → 0.2 µM Agatoxin IVA (*Aga4A*)

R-type → 0.2 µM SNX482 (*SNX*)

T-type → 5 µM ML218 + 30 µM NNC550396 (*ML+NNC*).

Fig. 4*A-C* shows three representative cells in which one type of HVA-VGCC (L-type, N-type or P/Q-type) was selectively blocked. All blockers produced a small broadening of the somatic action potential and a small reduction of both $\Delta F/F_0$ and I_{Ca}/Vol peaks in the proximal dendrite. Addition of the R-type channel blocker SNX-482 (Newcomb *et al.* 1998) slightly increased the $\Delta F/F_0$ signal in all regions (Fig. 4*D*). In contrast, the block of T-type VGCCs decreased the $\Delta F/F_0$ and I_{Ca}/Vol peaks in all regions, but more prominently in the distal region (Fig. 4*E*). Finally, the block of all VGCCs produced a deformation of the somatic action potential form and strongly decreased both $\Delta F/F_0$ and I_{Ca}/Vol peaks in all regions (Fig. 4*F*). The six representative examples shown in Fig. 4 were consistent with the statistical analysis performed on groups of 6-10 cells in which the effects of one selective inhibitor or of all the inhibitors together were tested (Table 1). In the proximal and medial regions, nearly half of the Ca^{2+} current is mediated by HVA-VGCCs with a dominance of L-type channels which are responsible of nearly a fourth of the total current. In the distal regions, addition of HVA-VGCCs blockers had negligible effect on the I_{Ca}/Vol signal suggesting that the Ca^{2+} current at these sites is almost exclusively mediated by the other channels. Surprisingly, SNX-482 did not reduce the I_{Ca}/Vol amplitude at any location. This toxin, however, also blocks A-type K^+ channels (Kimm & Bean, 2014) reducing the attenuation of the bAP along the apical dendrite and therefore enhancing the activation of the other channels that may compensate the loss of current mediated by R-type VGCCs. In agreement of this hypothesis, the block of all VGCCs decreased the I_{Ca}/Vol peak of ~90 % in all regions. Thus, the difference between the sum of the mean values of the I_{Ca}/Vol peak percentage changes produced by each individual blocker and the mean I_{Ca}/Vol peak percentage change produced by addition of all blockers is likely due to R-type channels. The residual ~10

% of the current after the concomitant block of all channels could be in principle due to Ca^{2+} release from stores, but in a previous study we have observed that this potential Ca^{2+} source does not contribute to the fast Ca^{2+} transient associated with the bAP (Jaafari *et al.* 2014). A second possibility is that this component is mediated by NMDA receptors bound to glutamate and blocked by Mg^{2+} that can be transiently unblocked by dendritic depolarisation (Santos *et al.* 2012). To explore this hypothesis we tested the effect of adding glutamate receptor antagonists NBQX (20 µM) and DL-AP5 (50 µM) on the Ca^{2+} transient and current. As shown in the example of Fig. *5A*, addition of glutamate receptors blockers did not change the Ca^{2+} transients and currents in the proximal, medial and distal regions. The same result was obtained in all 6 neurons where this test was performed (Table 1). We concluded that glutamate receptors do not contribute to the Ca^{2+} current associated with the bAP. Since it was shown that addition of $CdCl_2$ is capable to almost completely block the current (Jaafari *et al.* 2014), we also concluded that the residual ~10 % of the current shall be mainly mediated by VGCCs that are resistant to VGCCs blockers tested.

Ca^{2+} transients and currents associated with bursts

The experiments reported in the previous paragraph were performed by evoking a somatic action potential with a high-intensity (> 3 nA) current pulse of 1 ms duration and by averaging 16 trials after verifying that the action potential was consistent in all trials. Instead, in the cell of Fig. 6*A*, we evoked one action potential or bursts of 2-3 action potentials by injecting current pulses of 25 ms duration at different intensities (100-400 pA), and we analysed signals from single trials. In CA1 hippocampal pyramidal neurons, this type of burst can be evoked by distal dendritic plateau potentials *in vitro* (Takahashi & Magee, 2009) and *in vivo* (Grienberger *et al.* 2014), but it can also simply considered the response of the cell to the prolonged somatic depolarisation caused by multiple synaptic inputs. As shown in Fig. 6*B*, the shape of the action potential was different for the first spike in the three different stimulating protocols and for the three spikes in the burst of three action potentials. In particular, during the burst, the action potentials decreased in amplitude and increased in duration. Notably, in the proximal and medial regions, the $\Delta F/F_0$ signal associated with each action potential had the same amplitude whereas in the distal region the signal was variable. The $\Delta F/F_0$ signals for the three action potentials of the burst are shown in Fig. 6*C* which also reports the corresponding I_{Ca}/Vol signals. In the proximal and medial regions the I_{Ca}/Vol signals decreased in amplitude and increased in duration within the burst, although their integrals (i.e. the

$\Delta F/F_0$ signals) did not change in amplitude. In contrast, in this specific cell, the distal I_{Ca}/Vol signal increased in amplitude within the burst suggesting a phenomenon of regeneration similarly to what reported in the literature (Andreasen & Lambert, 2005). Remarkably, the behaviours of the $\Delta F/F_0$ and I_{Ca}/Vol signals in the proximal and medial regions was consistently observed in all the 12 cells in which we analysed bursts of three action potentials evoked by 25 ms current pulses (Fig. 6*D*). The statistical results of these experiments are reported in detail in Table 2. The changes of the second and third $\Delta F/F_0$ peak, with respect to the first one, were within 10% in each cell and not statistically significant. The stability of the Ca^{2+} transients during the burst was the consequence of a significant increase in duration of the Ca^{2+} current that compensated a significant decrease in amplitude. This behaviour was in contrast never observed in the distal region where both the $\Delta F/F_0$ and I_{Ca}/Vol signals were variable. The results illustrated in Fig. 6 and presented in Table 2 show that during a burst of action potentials the dendritic Ca^{2+} current associated with the spike changes its kinetics but preserves its integral resulting in the high-fidelity of Ca^{2+} elevation. This effect occurs only in the first 200 µm segment of the apical dendrite where, according to the pharmacological analysis reported in Table 1, HVA-VGCCs are always activated by the first bAP. The behaviour observed by evoking the burst with a pulse of 25 ms duration at low current intensity could be reproduced by evoking three action potentials with pulses of 1 ms duration at high intensity, as shown in the example of Fig. 7. In this experiment, we delivered the pulses either with a 8 ms interval or a 6 ms interval (Fig. 7*A*) and, in this way, we could average 16 recordings where the kinetics and the exact occurrence of the three action potentials were consistent. As shown in Fig. 7*B*, the amplitude of the individual Ca^{2+} transients associated with each action potential was the same in the proximal and medial regions. The corresponding I_{Ca}/Vol decreased in amplitude and increased in duration at both inter-spike intervals, but the effect was stronger when the action potentials were delivered at 6 ms interval (Fig. 7*C*). The Ca^{2+} current was therefore capable to tune its kinetics to preserve the amplitude of the Ca^{2+} elevation when the firing frequency changed. In the particular example reported in Fig. 7, in the distal region, the first action potential was associated with a Ca^{2+} signal below our resolution while small Ca^{2+} signals of different amplitude were observed at the second and third action potentials. As in the case of the example of Fig. 6, the distal I_{Ca}/Vol signal increased in amplitude within the train. The data analysis for this cell (reported in Fig. 7*D*) and for additional 6 cells (Fig. 8) show that in the proximal and medial regions the Ca^{2+} current is changing in amplitude and duration to consistently produce a stable Ca^{2+} signal. Therefore,

in the proximal and medial dendrite, the bAP reliably codes a precise Ca^{2+} signal independently of the interval between two consecutive action potentials in the burst, which is physiologically affected by stochastic fluctuations. In order to understand whether this phenomenon was coherently associated with the local change of membrane potential during the burst, we investigated the correlation between the bAPs waveform and the associated I_{Ca}/Vol signal in the case of three action potentials with 8 ms interval. In the particular example of Fig. 9*A-B*, the first bAP exhibited modest attenuation along the apical dendrite, and in all three regions the second and third bAPs had smaller amplitude with respect to the first one. As expected from the results reported in Figs. 6-8, a constant Ca^{2+} signal in the proximal and medial regions was obtained as result of the broadening and decrease in amplitude of the Ca^{2+} current waveform. In the other shown example of Fig. 9*D-E*, the first bAP attenuated more strongly along the apical dendrite with respect to the example of Fig. 9*A-B*. Also in this case, in the proximal and medial regions, the second and third bAPs had smaller amplitude with respect to the first one, but in the distal dendrite the depolarisation was stronger during the second and third event. Regardless of the different behaviour in the distal dendrite, the $\Delta F/F_0$ amplitude in the proximal and medial regions was again preserved as result of the compensation between the decrease in Ca^{2+} current amplitude and the increase in Ca^{2+} current duration. As shown in Fig. 9*E*, in 11 cells tested, the change in V_m peak was correlated with the change in I_{Ca}/Vol peak in the proximal region (Pearson coefficient $\rho = 0.43$, $p < 0.05$), in the medial region (Pearson coefficient $\rho = 0.61$, $p < 0.01$), and also in the distal region (Pearson coefficient $\rho = 0.90$, $p < 0.01$). Yet, in the proximal and medial region the second and third bAP and the second and third I_{Ca}/Vol peaks were consistently smaller than the first bAP and the first I_{Ca}/Vol peaks respectively. In the proximal and medial regions, but not in the distal region, the changes in V_m halfwidth were also correlated with the changes in I_{Ca}/Vol halfwidth (Pearson coefficients $\rho = 0.52$, $p < 0.05$ and $\rho = 0.54$, $p < 0.05$ respectively, Fig. 9*E*). Thus, the decrease in amplitude and the increase in duration of the Ca^{2+} currents in the proximal and medial dendrite were consistently associated with a similar change of the local V_m waveform. The combined analysis of the bAPs and of the I_{Ca}/Vol signals is illustrated in Fig. 9*F* and presented in Table 3. In particular, with respect to the first bAP, the second and third bAPs significantly decreased in amplitude and increased in duration in the proximal and medial regions. In the same regions, the second and third I_{Ca}/Vol peak significantly decreased with respect to the first one, but the decrease in I_{Ca}/Vol peak was compensated by an increase in duration. The result was that the integral of the I_{Ca}/Vol was preserved in

both regions and therefore the changes of the second and third $\Delta F/F_0$ peak with respect to the first one were not significant. The behaviour of both the V_m and Ca^{2+} optical signals in the distal region was instead highly variable from cell to cell. We can therefore conclude that the different behaviours of the Ca^{2+} signals associated with bAPs and bursts in the two distinct dendritic fields reflect the change in V_m waveform associated with the bAP.

A functional coupling of diverse VGCCs underlies the high-fidelity of Ca^{2+} signals

During somatic bursts of action potentials, the spikes progressively decrease in amplitude and increase in duration. As shown in Fig. 9, this change in the V_m waveform is enhanced as the action potentials propagate in the initial 200 µm dendritic segment while the distal signals are highly variable. It is known that the initial somatic decrease of action potentials is due to fast inactivation of Na^+ channels (Martina & Jonas, 1997) and the associated increase in duration is due to a weaker activation of K^+ channels, including Ca^{2+}-activated K^+ channels (Moyer *et al.* 1992; Tonini *et al.* 2013). Here, to precisely investigate the activation and de-activation of the different VGCCs during this change of the V_m waveform, we analysed the Ca^{2+} transient in the proximal dendrite while measuring the shape of the somatic action potentials, which are similar to the proximal bAPs (see Fig. 9). In the example of Fig. 10*A*, the third somatic action potential of a train at 8 ms interval is superimposed on the first one (see protocol of Fig. 9). The decrease in amplitude of the proximal current is likely due to the reduced activation of HVA-VGCCs while its increase in duration is likely due to prolonged activation of LVA-VGCCs. In line with this hypothesis, as shown in the example of Fig. 10*B*, the combined block of L-type and N-type channels by addition of Isradipine (20 µM) and PD173212 (5 µM) increased the duration of the somatic action potential and of the proximal Ca^{2+} current, but decreased the amplitude of the Ca^{2+} current. In contrast, as shown in the example of Fig. 10*C*, the block of LVA-VGCCs (T-type channels) by addition of ML218 (5 µM) and NNC550396 (30 µM) did not change the action potential waveform, but it decreased the amplitude and duration of the proximal Ca^{2+} current. The broadening of the somatic action potential associated with the block of HVA-VGCCs can be partially due to a weaker activation of Ca^{2+}-activated small K^+ (SK) channels (Jones & Stuart, 2013; Wang *et al.* 2014). As shown in the example of Fig. 10*D*, addition of Apamin (200 nM) indeed produced a small but detectable increase in the duration of both the somatic action potential and of the proximal Ca^{2+} current. As shown in the first statistics reported in Fig. 10*E*, the block of either L-

type and N-type channels or of SK channels increased the halfwidth of the action potential by 25 ± 17 % (N = 15, $p < 0.01$, paired t-test) and by 15 ± 6 % (N = 7, $p < 0.01$, paired t-test) respectively. This result indicates that part of the larger increase in the halfwidth of the action potential, with respect to the first one (43 ± 20 %, N = 18, $p < 0.01$, paired t-test) is due to the lack of activation of HVA-VGCCs and, as a consequence, of SK channels. The change in the action potential halfwidth, produced by the block of T-type channels (1 ± 7 %, N = 10 cells), was instead negligible. The pharmacological block of the different channels is however quantitatively different from their physiological modulation during the train. Thus, whereas the proximal Ca^{2+} transient associated with the third action potential negligibly changed with respect to the first one (+3 ± 5 %, N = 18 cells, Fig. 10*E*), the block of L-type and N-type channels or the block of T-type channels significantly decreased the $\Delta F/F_0$ signal by 21 ± 13 % (N = 15, $p < 0.01$, paired t-test) or by 24 ± 24 % (N = 10, $p < 0.05$, paired t-test) respectively. The block of SK channels, in contrast, slightly increased the $\Delta F/F_0$ signal by 26 ± 31 % (N = 7 cells). In the case of block of L-type and N-type channels, the increase in the I_{Ca}/Vol halfwidth by 26 ± 19 % ($p < 0.01$, paired t-test) did not compensate the decrease in the I_{Ca}/Vol peak by 40 ± 12 % ($p < 0.01$, paired t-test). In the case of block of T-type channels, the decrease of the Ca^{2+} transient was the combination of the decreases in I_{Ca}/Vol peak of 21 ± 23 % and in the I_{Ca}/Vol halfwidth of 7 ± 15 % respectively. Finally, the block of SK channels did not change the I_{Ca}/Vol peak (9 ± 22 %) while significantly increasing the I_{Ca}/Vol halfwidth by 15 ± 7 % ($p < 0.01$, paired t-test). The results obtained by this pharmacological analysis can only partially account for the complex molecular activation and de-activation of multiple channels responsible for the high fidelity of the Ca^{2+} signals during physiological bursts. Nevertheless, they demonstrate that the functional coupling between HVA-VGCCs and LVA-VGCCs is a central mechanism responsible for the tuning in amplitude and duration of the Ca^{2+} current that stabilises the Ca^{2+} elevation associated with the bAP when the V_m physiologically changes its waveform. In particular, VGGCs activate with a delay after their threshold for activation during the raising phase of the action potential and de-activate with a delay after the same threshold during the repolarisation. Several K^+ channels activate during the action potentials and, among those, SK channels are rapidly activated by the Ca^{2+} entered *via* HVA-VGCCs contributing to the repolarisation rate. Therefore, during action potential trains, a reduced activation of L- and N- type calcium channels decreases the K^+ current, slowing down the repolarisation and delaying the de-activation of T-type channels.

Discussion

The temporal information on the activation and de-activation of Ca^{2+} channels during physiological activity, i.e. the local measurement of Ca^{2+} currents, is beyond the ability of electrode techniques. This paper reports the first study of local dendritic Ca^{2+} currents during bAP activity based on direct optical measurements using a recent technique (Jaafari *et al.* 2014). We were able to monitor the kinetics of Ca^{2+} currents, delayed with respect to the depolarisation waveform (see Fig. 3*B*), and associate the global behaviour of the current to synergistic activation of HVA-VGCCs and LVA-VGCCs. In particular, we found that during somatic action potential firing the Ca^{2+} signal behave in a functionally different manner in the initial 200 µm of the apical dendrite (proximal and medial dendrite) and in its more distal parts. While somatic bursts in distal dendrites can be produced by distal dendritic depolarisation (Takahashi & Magee, 2009), the scenario described here in the initial 200 µm of the apical dendrite corresponds to a physiological somatic depolarisation produced by activation of sparse excitatory synaptic inputs.

In the proximal and medial dendrite, the bAP attenuates less than 50% and the peak of the V_m waveform is always above the threshold for activation of HVA-VGCCs. During a burst of action potentials, the decrease of Ca^{2+} influx *via* HVA-VGCCs due to the progressively reduced amplitude of the bAPs is replaced by a more prolonged influx of Ca^{2+} *via* LVA-VGCCs. The key mechanism permitting this precise tuning is the regulation of the duration of the bAP. Activation of Ca^{2+}-activated K^+ channels participates in coupling the amplitude of the L-type and N-type VGCCs current to the duration of the LVA-VGCCs current to stabilise the Ca^{2+} elevation associated with each bAP independently of its waveform. This scenario is a first approximation since it neglects P/Q-type channels, that may also regulate the duration of the action potential, and R-type channels, that can also prolong their period of opening. In addition, the broadening of the somatic action potentials caused by addition of Apamin was, on average, smaller than that caused by addition of L-type and N-type channels blockers. Therefore, the result of the specific contribution of SK channels should be considered preliminary with respect of the global contributions of K^+ channels. Hence, Ca^{2+}-activated big K^+ (BK) channels (Sun *et al.* 2003) and other K^+ channels are also expected to contribute to the Ca^{2+}-dependent repolarisation rate of the action potential. In the mouse, the proximal and medial dendritic segments represent more than 50 % of the total length. Notably, this zone corresponds to

the field of innervation of Shaffer collateral inputs from CA3 pyramidal neurons. In absence of paired synaptic inputs, the Ca^{2+} transient associated with the individual bAP is below the threshold for induction of synaptic potentiation but precise activation of dendritic proteins may contribute to plasticity mechanisms in combination with synaptic signalling. Further experimental analysis will be required to establish whether HVA-VGCCs are also activated by bAPs at the most distal sites of the oblique dendrites (Gasparini & Magee, 2006). Indeed, a large portion of Shaffer collateral contacts are formed on oblique branches where the bAP and the associated Ca^{2+} transient attenuate with the distance from the branching point (Gasparini *et al.* 2007). The stability of the Ca^{2+} transient associated with the bAP may be also important for triggering the production and release of second messengers, for instance endocannabinoids targeting pre-synaptic neurons (Wilson *et al.* 2001) and astrocytes (Navarrete & Araque, 2010). The dynamics of this process would be fast, but slower than the classical process of transmitter release at pre-synaptic terminals. Indeed, the current mediated by HVA-VGCCs has very short duration corresponding to the interval in which V_m is above their activation threshold, but delayed by a few hundred microseconds. The Ca^{2+} transient will therefore reach its peak after the termination of the current mediated by the more persistent LVA-VGCCs, typically > 1ms after the bAP peak.

The high-fidelity behaviour of single Ca^{2+} transients does not occur where HVA-VGCCs are not reliably activated by single bAPs, i.e. in distal dendrites located in the *stratum lacunosum moleculare*. In this area, bAPs do not always decrease monotonically but may change in amplitude within the burst. The correlation between the larger I_{Ca}/Vol signals and the associated larger depolarisation events (see the example in Fig. 9*D*) suggests that regenerative events involve activation of R-type channels and possibly of HVA-VGCCs. This variable Ca^{2+} signal is temporally locked to one or more bAPs within the burst, but its random occurrence during the bursts cannot provide a reliable indicator. The distal part of the dendrite, corresponding to the area of innervations of the perforant pathway, is also characterised by the ability to generate dendritic Ca^{2+} spikes (Golding *et al.* 2002) or of plateau potentials (Takahashi & Magee, 2009) that can replace bAPs for the induction of synaptic plasticity. It will be obviously interesting, in the future, to investigate the activity of different VGCCs during these events using our experimental approach. In these experiments, however, it will be necessary to discriminate the Ca^{2+} contribution of VGCCs from that of NMDA receptors, a task that is not straightforward under our experimental conditions. The information carried by Ca^{2+} signals associated with somatic firing activity in these two distinct functional areas of the

apical dendrite of the CA1 hippocampal pyramidal neuron has important implications in the way the cell can integrate and process the information from the Schaffer collateral input and from the perforant pathway. The attenuation of individual bAPs and the regeneration of distal dendritic depolarisation is a phenomenon also found in pyramidal neurons of the cortex and other cells. In neocortical layer-5 neurons (Larkum *et al.* 1999) and layer-6 pyramidal neurons (Laderberger & Larkum, 2010, for instance, short high-frequency bursts can elicit Ca^{2+} spikes in the dendritic tufts while the Ca^{2+} transient associated with single bAPs is highly variable. In all these systems, the dendritic site where the bAP fails to activate HVA-VGCCs will separate the dendritic fields into two functional areas: a proximal area where Ca^{2+} signals carry information on somatic firing at the level of single action potentials; and a distal area where Ca^{2+} signals reliably code only somatic bursts of action potentials. Interestingly in both cases mentioned, the two areas correspond to two different receptive synaptic fields.

References

Andreasen M & Lambert JD (1995) Regenerative properties of pyramidal cell dendrites in area CA1 of the rat hippocampus. *J Physiol* **483**, 421-441.

Bloodgood BL & Sabatini BL (2007) Nonlinear regulation of unitary synaptic signals by CaV(2.3) voltage-sensitive calcium channels located in dendritic spines. *Neuron* **53**, 249-260.

Canepari M & Mammano F (1999) Imaging neuronal calcium fluorescence at high spatio-temporal resolution. *J Neurosci Methods* **87**, 1 -11.

Canepari M & Odgen, D (2006) Kinetic, pharmacological and activity-dependent separation of two Ca^{2+} signalling pathways mediated by type 1 metabotropic glutamate receptors in rat Purkinje neurons. *J Physiol* **573**, 65-82.

Canepari M, Djurisic M & Zecevic D (2007) Dendritic signals from rat hippocampal CA1 pyramidal neurons during coincident pre- and post-synaptic activity: a combined voltage- and calcium-imaging study. *J Physiol* **580**, 463-484.

Canepari M & Vogt KE (2008) Dendritic Spike Saturation of Endogenous Calcium Buffer and Induction of Postsynaptic Cerebellar LTP. *PLoS ONE* **3**, e4011.

Canepari M, Vogt K & Zecevic D (2008) Combining voltage and calcium imaging from neuronal dendrites. *Cell Mol Neurobiol* **58**, 1079-1093.

Canepari M, Willadt S, Zecevic D & Vogt KE (2010) Imaging Inhibitory Synaptic Potentials Using Voltage Sensitive Dyes. *Biophys J* **98**, 2032-2040.

Christie BR, Eliot LS, Ito K, Miyakawa H & Johnston D (1995) Different Ca2+ channels in soma and dendrites of hippocampal pyramidal neurons mediate spike-induced Ca2+ influx. *J Neurophysiol* **73**, 2553-2557.

Frick A, Magee J & Johnston D (2004) LTP is accompanied by an enhanced local excitability of pyramidal neuron dendrites. *Nat Neurosci* **7**, 126–135.

Gasparini S, Losonczy A, Chen X, Johnston D & Magee JC (2007) Associative pairing enhances action potential back-propagation in radial oblique branches of CA1 pyramidal neurons. *J Physiol* **580**, 787-800.

Gasparini S & Magee JC (2006) State-dependent dendritic computation in hippocampal CA1 pyramidal neurons. *J Neurosci* **26**, 2088-20100.

Golding NL, Kath WL & Spruston N (2001) Dichotomy of action-potential backpropagation in CA1 pyramidal neuron dendrites. *J Neurophysiol* **86**, 2998-3010.

Golding NL, Staff NP & Spruston N (2002) Dendritic spikes as a mechanism for cooperative long-term potentiation. *Nature* **418**, 326-331.

Grienberger C, Chen X & Konnerth A (2014) NMDA receptor-dependent multidendrite Ca(2+) spikes required for hippocampal burst firing in vivo. *Neuron* **81**, 1274-1281.

Higley MJ & Sabatini BL (2008) Calcium signaling in dendrites and spines: practical and functional considerations. *Neuron* **59**, 902-913.

Hoffman DA, Magee JC, Colbert CM & Johnston D (1997) K+ channel regulation of signal propagation in dendrites of hippocampal pyramidal neurons. *Nature* **387**, 869–875.

Isaacson JS (2001) Mechanisms governing dendritic gamma-aminobutyric acid (GABA) release in the rat olfactory bulb. *Proc Natl Acad Sci USA* **98**, 337-342.

Jaafari N, De Waard M & Canepari M (2014) Imaging Fast Calcium Currents beyond the Limitations of Electrode Techniques. *Biophys J* **107**, 1280-1288.

Jaafari N, Marret E & Canepari M (2015) Using simultaneous voltage and calcium imaging to study fast Ca2+ channels. *Neurophotonics* **2**, 021010.

Jones SL & Stuart GJ (2013) Different calcium sources control somatic versus dendritic SK channel activation during action potentials. *J Neurosci* **33**, 19396-19405.

Kimm T & Bean BP (2014) Inhibition of A-type potassium current by the peptide toxin SNX-482. *J Neurosci* **34**, 9182-9189.

Ledergerber D & Larkum ME (2010) Properties of layer 6 pyramidal neuron apical dendrites. *J Neurosci* **30**, 13031-13044.

Larkum ME, Kaiser KM & Sakmann B (1999a) Calcium electrogenesis in distal apical dendrites of layer 5 pyramidal cells at a critical frequency of back-propagating action potentials. *Proc Natl Acad Sci USA* **96**, 14600–14604.

Lee G, Stewart R, Canepari M & Capogna M (2014) Firing of hippocampal neurogliaform cells induces suppression of synaptic inhibition. *J Neurosci* **34**, 1280-1292.

Magee JC & Johnston D (1995) Characterization of single voltage-gated sodium and calcium channels in the apical dendrites of rat CA1 pyramidal neurons. *J Physiol* **487**, 67–90.

Magee J, Hoffman D, Colbert C & Johnston D (1998) Electrical and calcium signaling in dendrites of hippocampal pyramidal neurons. *Annu Rev Physiol* **60**, 327-346.

Markram H, Helm PJ & Sakmann B (1995) Dendritic calcium transients evoked by single back-propagating action potentials in rat neocortical pyramidal neurons. *J Physiol* **485**, 1-20.

Martina M & Jonas P (1997) Functional differences in Na+ channel gating between fast-spiking interneurones and principal neurones of rat hippocampus. *J Physiol* **505**, 593-603.

Migliore M, Hoffman DA, Magee JC & Johnston D (1999) Role of an A-type K+ conductance in the back-propagation of action potentials in the dendrites of hippocampal pyramidal neurons. *J Comput Neurosci* **7**, 5-15.

Moyer JR Jr, Thompson LT, Black JP & Disterhoft JF (1992) Nimodipine increases excitability of rabbit CA1 pyramidal neurons in an age- and concentration-dependent manner. *J Neurophysiol* **68**, 2100-2109.

Navarrete M & Araque A (2010) Endocannabinoids potentiate synaptic transmission through stimulation of astrocytes. *Neuron* **68**, 113-126.

Newcomb R, Szoke B, Palma A, Wang G, Chen Xh, Hopkins W, Cong R, Miller J, Urge L, Tarczy-Hornoch K, Loo JA, Dooley DJ, Nadasdi L, Tsien RW, Lemos J & Miljanich G (1998) Selective peptide antagonist of the class E calcium channel from the venom of the tarantula Hysterocrates gigas. *Biochemistry* **37**, 15353-15362.

Sabatini BL & Regehr WG (1998) Optical measurement of presynaptic calcium currents. *Biophys J* **74**, 1549-1563.

Santos MD, Mohammadi MH, Yang S, Liang CW, Kao JP, Alger BE, Thompson SM & Tang CM (2012) Dendritic hold and read: a gated mechanism for short term information storage and retrieval. *PLoS One* **7**, e37542.

Spruston N, Schiller Y, Stuart G & Sakmann B (1995) Activity-dependent action potential invasion and calcium influx into hippocampal CA1 dendrites. *Science* **268**, 297-300.

Sun X, Gu XQ, Haddad GC (2003) Calcium influx via L- and N-type calcium channels activates a transient large-conductance Ca2+-activated K+ current in mouse neocortical pyramidal neurons. *J Neurosci* **23**, 3639-36348.

Takahashi H & Magee JC (2009) Pathway interactions and synaptic plasticity in the dendritic tuft regions of CA1 pyramidal neurons. *Neuron* **62**, 102-111.

Tonini R, Ferraro T, Sampedro-Castañeda M, Cavaccini A, Stocker M, Richards CD & Pedarzani P (2013) Small-conductance Ca2+-activated K+ channels modulate action potential-induced Ca2+ transients in hippocampal neurons. *J Neurophysiol* **109**, 1514-1524.

Vogt KE, Gerharz S, Graham J & Canepari M (2011a) High-resolution simultaneous voltage and Ca^{2+} imaging. *J Physiol* **589**, 489-494.

Vogt KE, Gerharz S, Graham J & Canepari M (2011b) Combining membrane potential imaging with L-glutamate or GABA photorelease. *PLoS ONE 6*, e24911.

Wang K, Lin MT, Adelman JP & Maylie J (2014) Distinct Ca2+ sources in dendritic spines of hippocampal CA1 neurons couple to SK and Kv4 channels. *Neuron* **81**, 379-387.

Waters J, Schaefer A & Sakmann B (2005) Backpropagating action potentials in neurones: measurement, mechanisms and potential functions. *Prog Biophys Mol Biol* **87**, 145-170.

Williams SR & Stuart GJ (2000) Backpropagation of physiological spike trains in neocortical pyramidal neurons: implications for temporal coding in dendrites. *J Neurosci* **20**, 8238-8246.

Wilson RI, Kunos G & Nicoll RA (2001) Presynaptic specificity of endocannabinoid signaling in the hippocampus. *Neuron* **31**, 453-462.

Yasuda R, Nimchinsky EA, Scheuss V, Pologruto TA, Oertner TG, Sabatini BL & Svoboda K (2004) Imaging calcium concentration dynamics in small neuronal compartments. *Sci STKE* **3** 219, pl5.

Additional information

Competing interests

None

Author contributions

N.J. and M.C. designed the study, performed the experiments, analysed the data and wrote the paper.

Funding

This work was supported by the *Agence Nationale de la Recherche* through three grants: 1. Labex *Ion Channels Science and Therapeutics*, program number ANR-11-LABX-0015; 2. National Infrastructure France Life Imaging “Noeud Grenoblois” ; 3. Grant *WaveFrontImag*, program number ANR-14-CE17-0006-01 and by the *Federation pour la recherché sur le Cerveau* (FRC) through the grant *Espoir en tête* (in partnership with Rotary France).

Acknowledgements

We thank Elodie Marret for technical help and Kaspar Vogt for reading the manuscript before submission.

	Isradipine (N = 8)	PD173212 (N = 7)	Agatoxin IVA (N = 6)	SNX-482 (N = 6)	ML218 + NNC550396 (N = 10)	All VGGCs blockers (N = 6)	NBQX + DL-AP5 (N = 6)
Ca^{2+}-ΔF/F_0 P	-5 ± 7 %	-11 ± 12 %	-3 ± 6 %	4 ± 4 %	-24 ± 24 %*	-72 ± 10 %* *	2 ± 4 %
Ca^{2+}-ΔF/F_0 M	-2 ± 9 %	-7 ± 10 %	3 ± 11 %	15 ± 13 %,	-30 ± 24 %*	-72 ± 18 %**	1 ± 4 %,
Ca^{2+}-ΔF/F_0 D	7 ± 18 %	2 ± 9 %	0 ± 4 %	15 ± 17 %	-52 ± 41 %**	-78 ± 8 %**	-2 ± 6 %
I_{Ca}/Vol P	-24 ± 13 %**	-15 ± 13 %	-10 ± 8 %*	-5 ± 10 %	-21 ± 23 %*	-86 ± 8 %**	1 ± 6 %
I_{Ca}/Vol M	-15 ± 15 %*	-10 ± 9 %	-8 ± 5 %*	0 ± 10 %	-22 ± 20 %**	-85 ± 11 %**	2 ± 5 %
I_{Ca}/Vol D	-2 ± 20 %	-2 ± 11 %	-6 ± 7 %	10 ± 16 %	-51 ± 44 %*	-90 ± 6 %**	-3 ± 9 %

Table 1. Results of the pharmacological analysis

Percentage change (mean ± SD) of the Ca^{2+}-ΔF/F_0 and of the I_{Ca}/Vol in P, M and D regions after addition of 20 µM Isradipine (*N = 8 cells*), 5 µM PD173212 (*N = 7 cells*), 0.2 µM Agatoxin IVA (*N = 6 cells*), 0.2 µM SNX-482 (*N = 6 cells*), 5 µM ML218 + 30 µM NNC550396 (*N = 10 cells*), all VGCCs blockers (*N = 6 cells*) or 20 µM NBQX + 50 µM DL-AP5. "*" means $p < 0.05$ in the paired t-test. "**" means $p < 0.01$ in the paired t-test. The analysis was performed on averages of 16 trials.

	Proximal	Medial	Distal
$2^{nd}/1^{st}$ Ca^{2+}-ΔF/F_0 peak	-3 ± 4 %	-5 ± 6 %	24 ± 90 %
$2^{nd}/1^{st}$ I_{Ca}/Vol peak	-13 ± 4 %**	-19 ± 10 %**	24 ± 80 %
$2^{nd}/1^{st}$ I_{Ca}/Vol ½width	13 ± 8 %**	17 ± 16 %**	-8 ± 21 %
$3^{rd}/1^{st}$ Ca^{2+}-ΔF/F_0 peak	0 ± 5 %	1 ± 11 %	50 ± 110 %
$3^{rd}/1^{st}$ I_{Ca}/Vol peak	-21 ± 10 %**	-26 ± 15 %**	41 ± 97 %
$3^{rd}/1^{st}$ I_{Ca}/Vol ½width	26 ± 13 %**	33 ± 13 %**	-1 ± 35 %

Table 2. Ca^{2+} currents associated with bursts of action potentials: analysis of 12 cells

From 12 cells, percentage change with respect to the first event (mean ± SD) of the second and third Ca^{2+}-ΔF/F_0 peak, I_{Ca}/Vol peak and I_{Ca}/Vol halfwidth in P, M and D regions during burst of three action potentials elicited by a long pulse of depolarizing current injection. "**" means $p < 0.01$ in the paired t-test. The analysis was performed on single trials.

	Proximal	Medial	Distal
$2^{nd}/1^{st}$ bAP peak	-11 ± 4 %**	-11 ± 4 %**	17 ± 78 %
$2^{nd}/1^{st}$ bAP ½width	19 ± 11 %**	17 ± 10 %**	-2 ± 14 %
$2^{nd}/1^{st}$ Ca^{2+}-$\Delta F/F_0$ peak	-1 ± 4 %	-5 ± 11 %	17 ± 145 %
$2^{nd}/1^{st}$ I_{Ca}/Vol peak	-15 ± 3 %**	-13 ± 6 %**	13 ± 129 %
$2^{nd}/1^{st}$ I_{Ca}/Vol ½width	13 ± 6 %**	13 ± 9 %**	10 ± 40 %
$3^{rd}/1^{st}$ bAP peak	-15 ± 5 %**	-13 ± 5 %**	15 ± 45 %
$3^{rd}/1^{st}$ bAP ½width	51 ± 19 %**	53 ± 28 %**	7 ± 15 %
$3^{rd}/1^{st}$ Ca^{2+}-$\Delta F/F_0$ peak	4 ± 5 %	-2 ± 6 %	26 ± 95 %
$3^{rd}/1^{st}$ I_{Ca}/Vol peak	-23 ± 7 %**	-18 ± 6 %**	29 ± 115 %
$3^{rd}/1^{st}$ I_{Ca}/Vol ½width	28 ± 7 %**	29 ± 10 %**	3 ± 38 %

Table 3. bAP trains and associated Ca^{2+} signals and currents along the apical dendrite: analysis of 11 cells. From 11 cells, percentage change with respect to the first event (mean ± SD) of the second and third bAP peak, bAP halfwidth, Ca^{2+}-$\Delta F/F_0$ peak, I_{Ca}/Vol peak and I_{Ca}/Vol halfwidth in P, M and D regions during trains of three action potentials elicited by short pulse of depolarising current injections at 8 ms interval. "**" means $p < 0.01$ in the paired t-test. The analysis was performed on averages of 9 trials.

Figure Legends

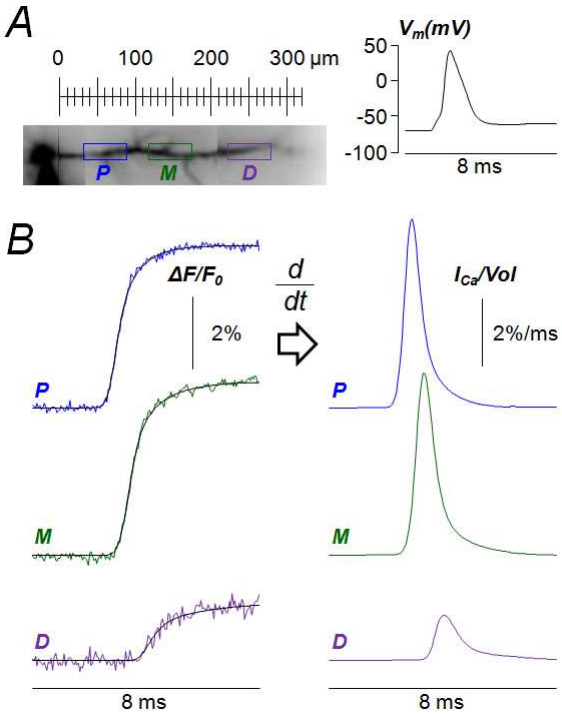

Figure 1. Ca^{2+} current to volume ratio (I_{Ca}/Vol) along the apical dendrite calculated as time derivative of the Ca^{2+}-$\Delta F/F_0$ signal.

A, On the left, the fluorescence reconstruction of a CA1 hippocampal pyramidal neuron with a proximal region (P), a medial region (M) and a distal region (D) indicated. On the right, the recording of a somatic action potential. *B,* On the left, the Ca^{2+}-$\Delta F/F_0$ signals in the P, M and D regions are fitted with 3-sigmoid functions as described in the Methods. On the right, the kinetics of the Ca^{2+} currents are obtained as the time derivatives of the fitted curves expressed in %/ms. Data were from averages of 16 trials.

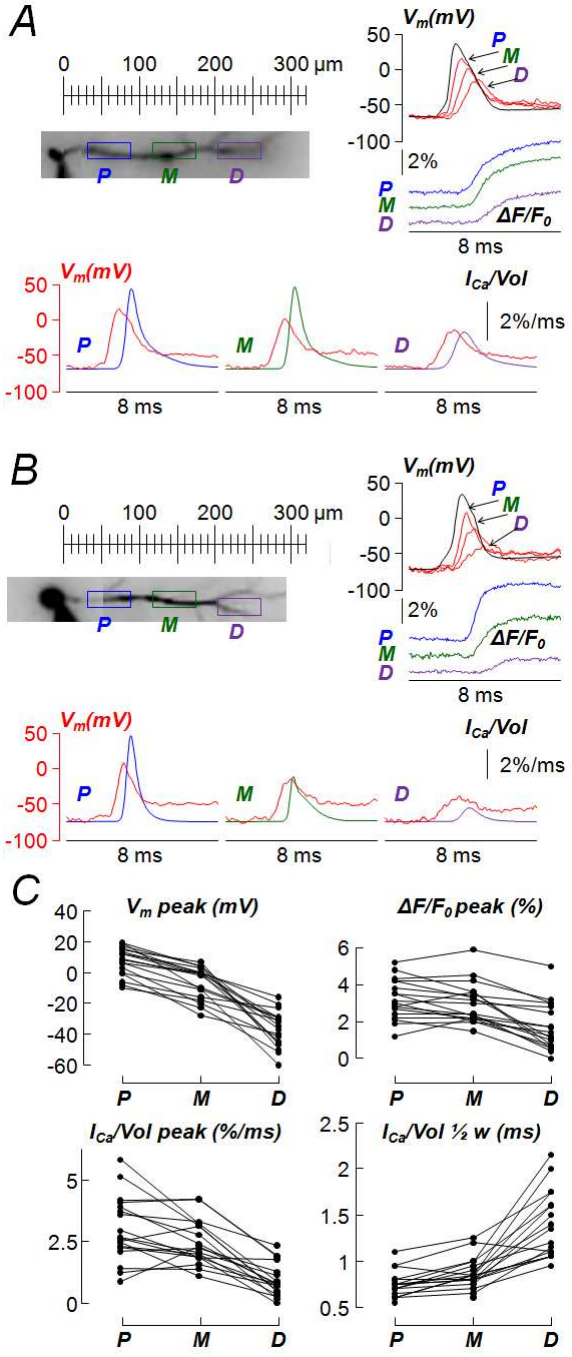

Figure 2. Single bAPs and the associated Ca^{2+} signal and current along the apical dendrite.

A-B, V_m change (red traces), Ca^{2+}-$\Delta F/F_0$ and I_{Ca}/Vol signals associated with a bAP along the apical dendrite from two representative CA1 hippocampal pyramidal neurons. Optical signals are from P, M and D dendritic regions indicated in the fluorescence image of the cell on the top-left panel. The black traces on right panels are the somatic recordings. Data were from averages of 9 trials. *C,* Plots of the V_m peak, of Ca^{2+}-$\Delta F/F_0$ peak, of the I_{Ca}/Vol peak and of the I_{Ca}/Vol halfwidth associated with a bAP along P, M and D regions from 18 cells. All data were from averages of 9 trials.

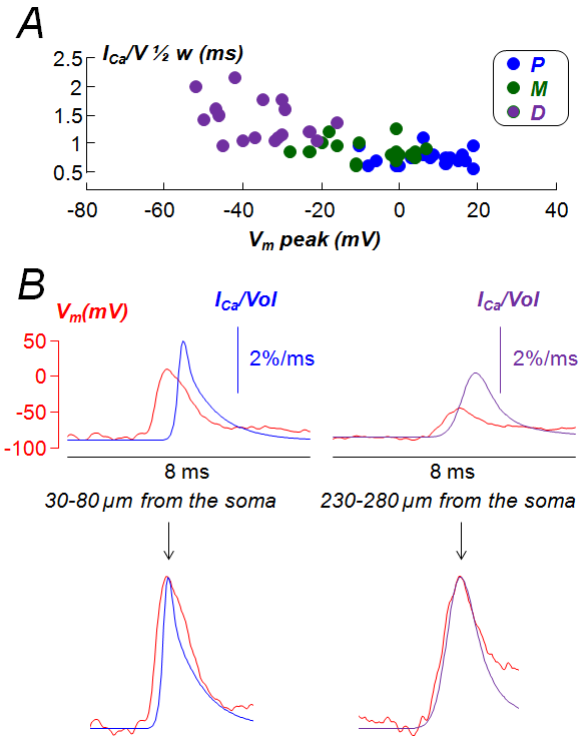

Figure 3. Correlation between the kinetics of the bAP and the kinetics of the Ca^{2+} current.

A, Plot of the I_{Ca}/Vol halfwidth against the local peak of bAP from 18 cells: black, blue and green points are from P, M and D regions respectively. The ensamble of points are negatively correlated (Pearson coefficient ρ=-0.70, $p < 0.01$). B, An example kinetics of the bAP and of the associated I_{Ca}/Vol in the proximal and in the distal dendrite. In the traces below, the two signals were aligned and normalised to their peak. The kinetics of the local bAP is similar to the kinetics of the I_{Ca}/Vol in the distal but not in the proximal dendrite.

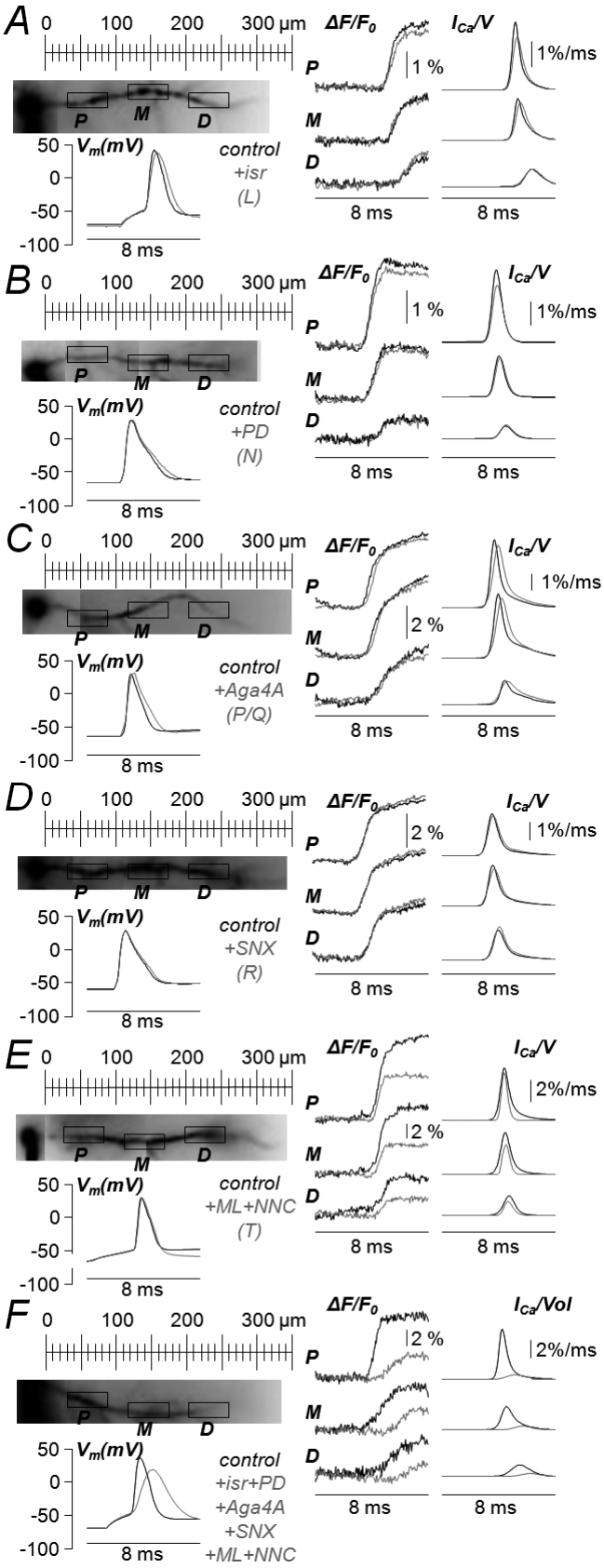

Figure 4. Effects of blocking of diverse VGCCs.

A-E, In the top-left panel the fluorescence reconstruction of a CA1 hippocampal pyramidal neuron with P, M and D regions of interest indicated. In the bottom-left panel the somatic action potential in control conditions (black trace) and after the addition of a VGCCs blocker (gray trace). In the right panel the Ca^{2+}-$\Delta F/F_0$ and I_{Ca}/Vol signals in control conditions (black trace) and after the addition of a VGCCs blocker (gray trace). Blockers used for this test were: (*A*) 20 µM Isradipine (*Isr*), (*B*) 5 µM PD173212 (*PD*), (*C*) 0.2 µM Agatoxin IVA (*Aga4A*), (*D*) 0.2 µM SNX-482 (*SNX*) and (*E*) 5 µM ML218 + 30 µM NNC550396 (*ML+NNC*). All data were from averages of 16 trials. *F*, In the top-left panel the fluorescence reconstruction of a CA1 hippocampal pyramidal neuron with P, M and D regions of interest indicated. In the bottom-left panel the somatic action potential in control conditions (black trace) and after the addition all VGCC blockers individually tested in *A-E* (gray trace). In the right panel the Ca^{2+}-$\Delta F/F_0$ and I_{Ca}/Vol signals in control conditions (black trace) and after the addition all VGCC blockers individually tested in *A-E* (gray trace). Data were from averages of 16 trials.

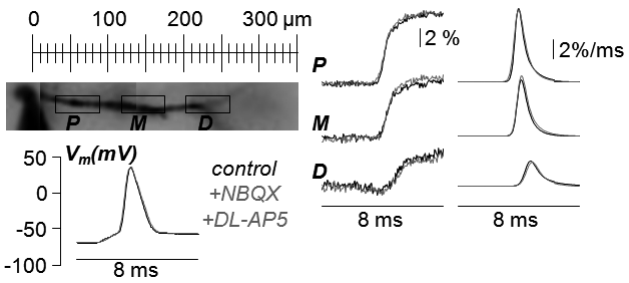

Figure 5. Effects of blocking glutamate receptors.

In the top-left panel the fluorescence reconstruction of a CA1 hippocampal pyramidal neuron with P, M and D regions of interest indicated. In the bottom-left panel the somatic action potential in control conditions (black trace) and after the addition of 20 µM NBQX and 50 µM DL-AP5 (gray trace). In the right panel the Ca^{2+}-$\Delta F/F_0$ and I_{Ca}/Vol signals in control conditions (black trace) and after the addition of 20 µM NBQX and 50 µM DL-AP5 (gray trace). Data were from averages of 16 trials.

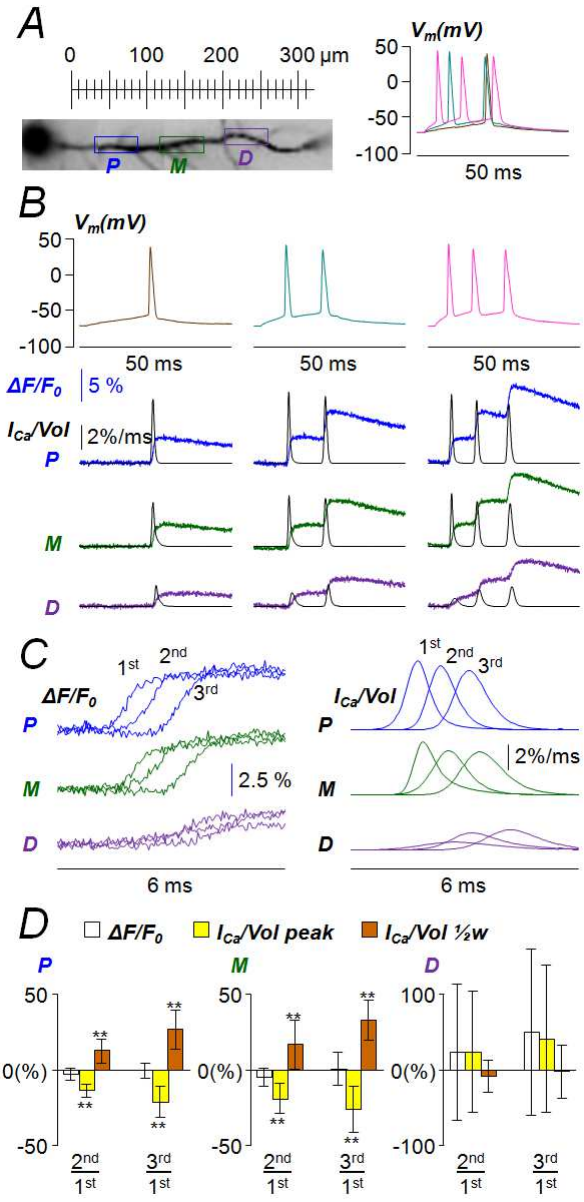

Figure 6. The Ca^{2+} currents associated with bursts of action potentials.

A, In the left panel the fluorescence reconstruction of a CA1 hippocampal pyramidal neuron with P, M and D regions of interest indicated. In the right panel the somatic recording in current clamp in response to injections of depolarising pulses of 25 ms at three different intensities (coloured traces). Data were from single trials. *B,* The three action potential patterns in A (top) aligned with the associated Ca^{2+}-$\Delta F/F_0$ and I_{Ca}/Vol signals (bottom) in the P, M and D regions. *C,* From the pattern with three action potentials elicited by the current pulse the three Ca^{2+}-$\Delta F/F_0$ transients (left) and I_{Ca}/Vol events (right) superimposed. *D,* Statistics (mean ± SD, N = 12 cells) of the ratios of the second or the third Ca^{2+}-$\Delta F/F_0$ peaks with respect to the first one, of the ratios of the second or the third I_{Ca}/Vol peaks with respect to the first one, of the ratios of the second or the third I_{Ca}/Vol halfwidths with respect to the first one. "*" means $p < 0.05$ in paired t-test. "**" means $p < 0.01$ in paired t-test. All results were from single trials.

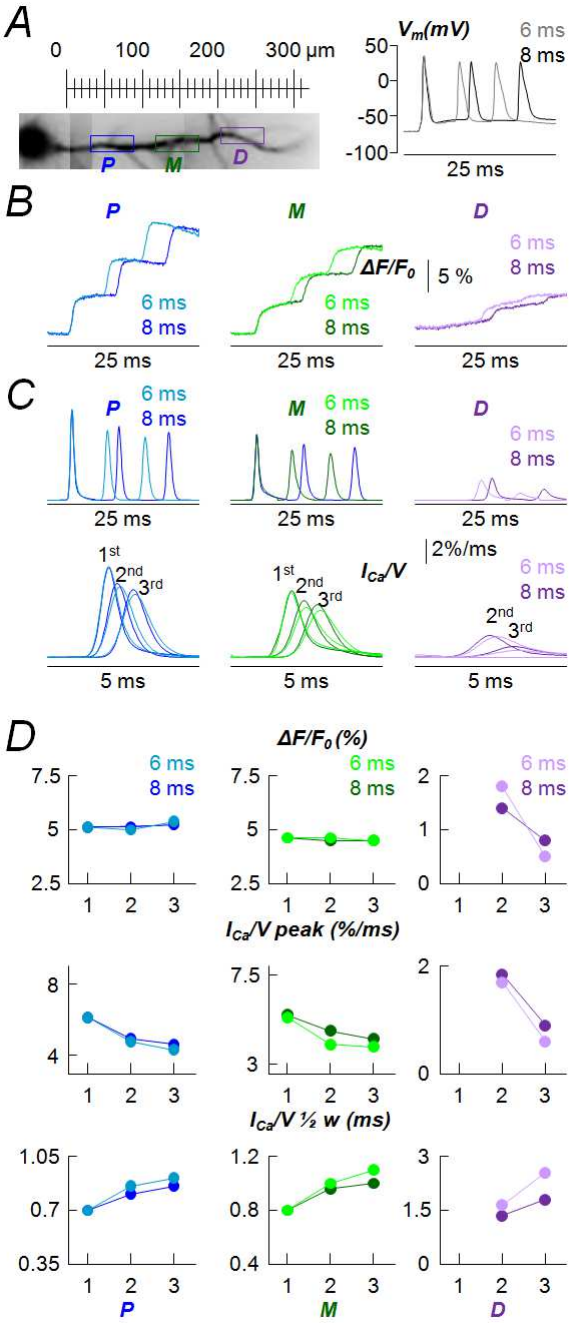

Figure 7. Ca^{2+} currents associated with trains of three action potentials at 8 ms and 6 ms interval.

A, In the left panel the fluorescence reconstruction of a CA1 hippocampal pyramidal neuron with P, M and D regions of interest indicated. In the right panel the somatic recording of three action potentials at 8 ms interval (black trace) and at 6 ms interval (gray trace). Data were from averages of 16 trials. *B,* Ca^{2+}-$\Delta F/F_0$ signals associated with the patterns of three action potentials at 8 ms interval and at 6 ms interval in the P, M and D regions. *C,* On the top, the I_{Ca}/Vol signal associated with the patterns of three action potentials at 8 ms interval and at 6 ms interval in the P, M and D regions. On the bottom, the same I_{Ca}/Vol events at 8 ms interval and at 6 ms interval aligned. *D,* From the same experiments, time course of the Ca^{2+}-$\Delta F/F_0$ amplitudes (plots in the top row), of the I_{Ca}/Vol peak (plots in the middle row) and of the I_{Ca}/Vol halfwidth (plots in the bottom row) as a function of the action potential number in the train. Left, centre and right columns correspond to the P, M and D regions respectively.

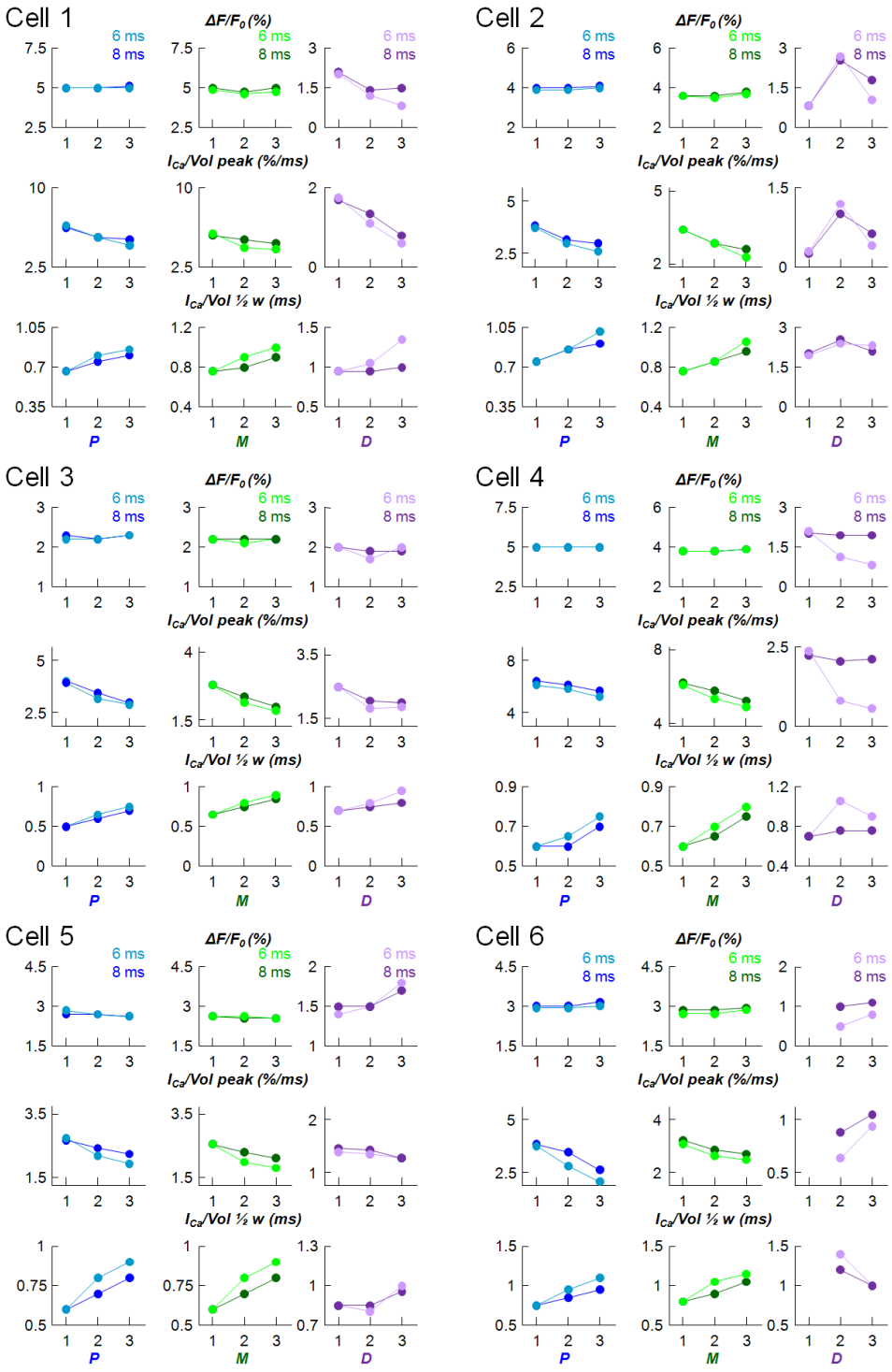

Figure 8. Ca^{2+} currents associated bursts of three action potentials at 8 ms and 6 ms interval: analysis of 6 cells.

For each cell, time course of the Ca^{2+}-$\Delta F/F_0$ amplitudes (plots in the top row), of the I_{Ca}/Vol peak (plots in the middle row) and of the I_{Ca}/Vol halfwidth (plots in the bottom row) as a function of the action potential number in the train. Left, centre and right columns correspond to the P, M and D regions respectively. Results were from averages of 16 trials.

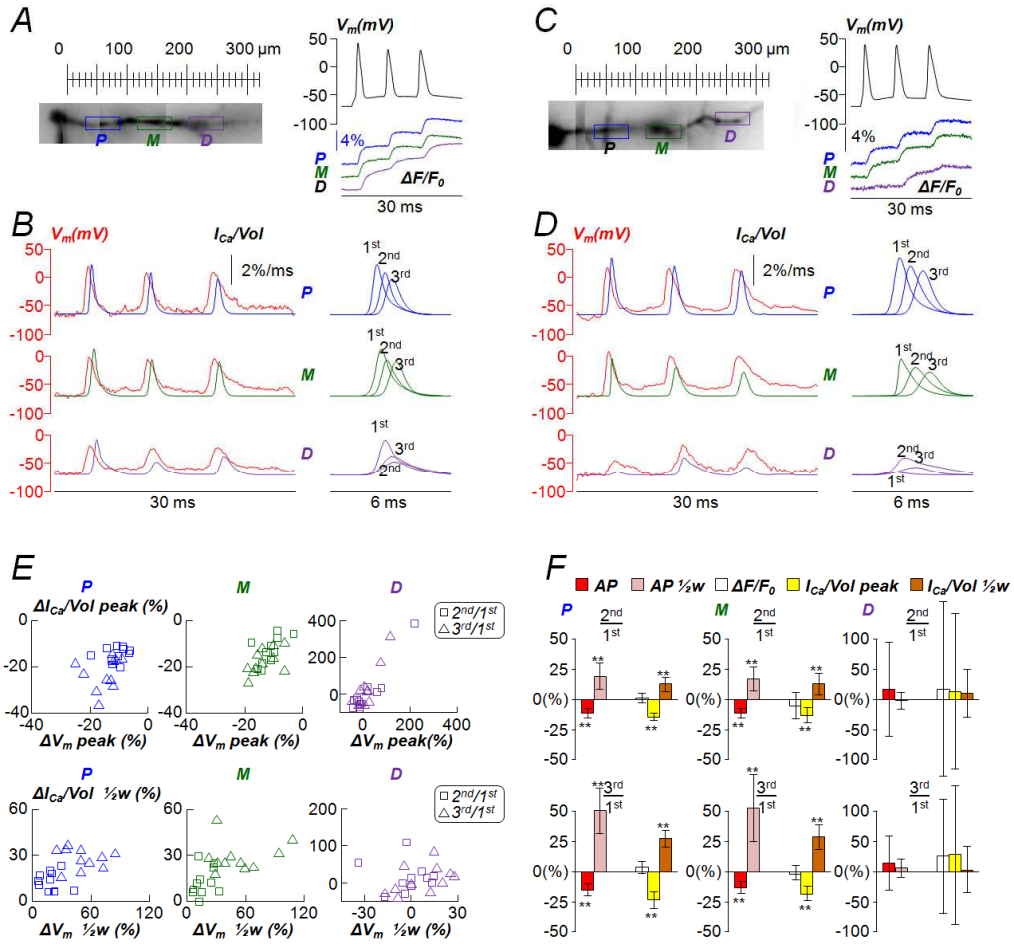

Figure 9. bAP trains and associated Ca^{2+} signals and currents along the apical dendrite.

A, In the left panel the fluorescence reconstruction of a CA1 hippocampal pyramidal neuron with P, M and D regions of interest indicated. In the right panel the somatic recording of three action potentials at 8 ms interval (top) and the associated Ca^{2+}-$\Delta F/F_0$ signals (bottom-right) in the P, M and D regions. Data were from averages of 9 trials. *B,* In the left panel, the three bAPs (red) and associated I_{Ca}/Vol in the P, M, and D regions from the same experiment. On the right, the same three I_{Ca}/Vol events in the P, M and D regions aligned. *C-D,* Same as A-B but from another neuron exhibiting stronger attenuation of the first bAP. *E,* In the top panel, plots of percentage change of the second (square symbols) and third (triangle symbols) I_{Ca}/Vol peak changes relative to the first I_{Ca}/Vol peak against the percentage changes of the bAP peak in the P, M and D regions. The plots were obtained from 11 cells using the same protocol of the cells in *A-B* and in *C-D*. Results were from averages of 9 trials. *F,* From the same experiments reported in E, statistics (mean ± SD) of the ratios between the second or third Ca^{2+}-$\Delta F/F_0$ peaks and the first one, of the ratios between the second or third I_{Ca}/Vol peaks and the first one, of the ratios between the second or third I_{Ca}/Vol halfwidths and the first one. "*" means $p < 0.05$ in paired t-test. "**" means $p < 0.01$ in paired t-test.

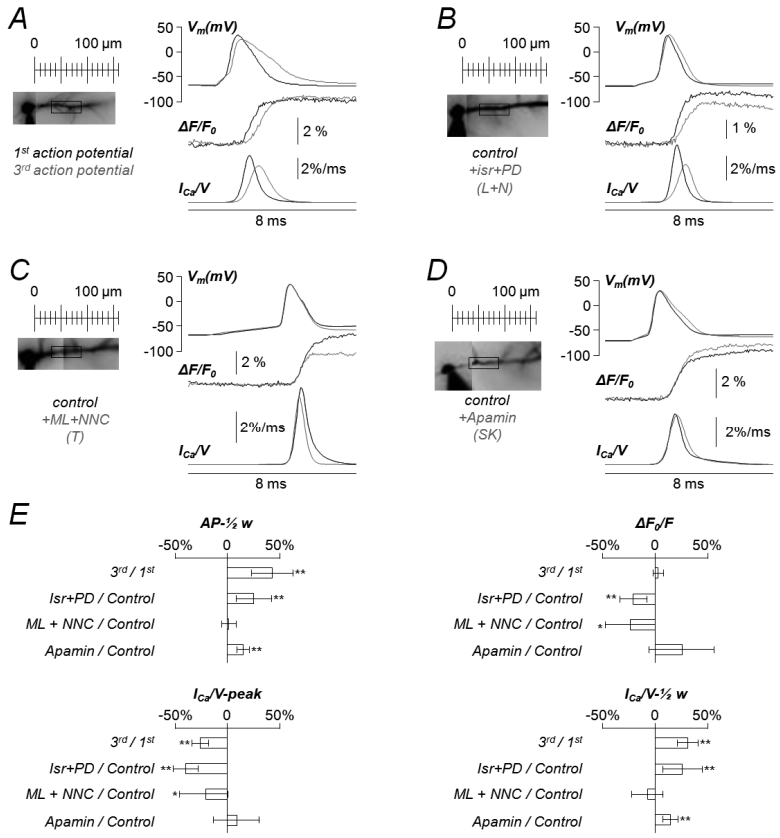

Figure 10. Functional coupling of the different VGCCs. *A,* On the left the fluorescence reconstruction of a CA1 hippocampal pyramidal neuron with a proximal region of interest indicated. The protocol of induction of three action potentials at 8 ms interval was delivered to this cell. On the top-right the somatic recording of first (black trace) and third (gray trace) action potential superimosed. On the bottom-right the associated Ca^{2+}-$\Delta F/F_0$ and I_{Ca}/Vol signals. Data were from averages of 16 trials. *B-D,* On the left of each panel the fluorescence reconstruction of a CA1 hippocampal pyramidal neuron with a proximal region of interest indicated. On the top-right of each panel the somatic recording of an action potential in control conditions (black trace) and after addition of channel blockers (gray trace). On the bottom-right of each panel the associated Ca^{2+}-$\Delta F/F_0$ and I_{Ca}/Vol signals. Blockers used for this test were: (*B*) 20 µM Isradipine + 5 µM PD173212 (*Isr+PD*), (*C*) 5 µM ML218 + 30 µM NNC550396 (*ML+NNC*) and (*D*) 0.2 µM Apamin. Data were from averages of 16 trials. *E,* Statistics (mean ± SD) of the change in the somatic action potential halfwidth, in the Ca^{2+}-$\Delta F/F_0$ peak, in the I_{Ca}/Vol peak and in the I_{Ca}/Vol halfwidth in the following protocols: third event with respect to first event in a train of action potentials at 8 ms interval (N = 18 cells); after addition of Isr+PD (N = 15 cells); after addition of ML+NNC (N = 10 cells); after addition of Apamin (N = 7 cells). "*" means $p < 0.05$ in the paired (control/blocker) t-test. "**" means $p < 0.01$ in the paired (control/blocker) t-test. All results were from averages of 16 trials.